ACS Catalysis

Research Article

Cite This: ACS Catal. 2018, 8, 7952−7960

pubs.acs.org/acscatalysis

Water-Nucleophilic Attack Mechanism for the $Cu^{II}(pyalk)_2$ Water-Oxidation Catalyst

Benjamin Rudshteyn, Katherine J. Fisher, Hannah M. C. Lant, Ke R. Yang, Brandon Q. Mercado, Gary W. Brudvig,* Robert H. Crabtree,* and Victor S. Batista*

Department of Chemistry and Energy Sciences Institute, Yale University, New Haven, Connecticut 06520, United States

Supporting Information

ABSTRACT: We investigate the mechanism of water oxidation catalyzed by the $Cu^{II}(pyalk)_2$ complex, combining density functional theory with experimental measurements of turnover frequencies, UV−visible spectra, H/D kinetic isotope effects (KIEs), electrochemical analysis, and synthesis of a derivative complex. We find that only in the *cis* form does $Cu^{II}(pyalk)_2$ convert water to dioxygen. In a series of alternating chemical and electrochemical steps, the catalyst is activated to form a metal oxyl radical species that undergoes a water-nucleophilic attack defining the rate-limiting step of the reaction. The experimental H/D KIE (3.4) is in agreement with the calculated value (3.7), shown to be determined by deprotonation of the substrate nucleophile upon O−O bond formation. The reported mechanistic findings are particularly valuable for rational design of complexes inspired by $Cu^{II}(pyalk)_2$.

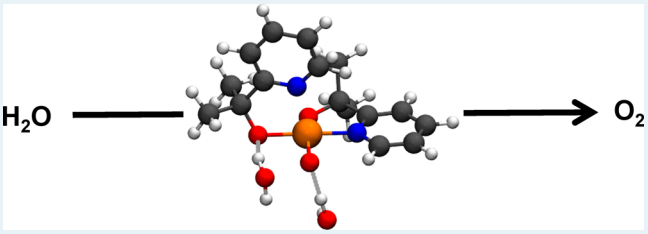

KEYWORDS: *water oxidation, catalysis, copper, water-nucleophilic attack, density functional theory, electrocatalysis*

INTRODUCTION

Catalytic water oxidation is a critical bottleneck in the generation of solar fuels, a challenging reaction that requires powerful and robust catalysts.[1] Transition metal catalysts require ligands that can stabilize high oxidation states and, at the same time, resist degradation under the harsh oxidative conditions.[2−4] We have found that the ligand 2-(2′-pyridyl)-2-propanoate (pyalk) is an exceptionally apt chelate that fulfills these requirements, forming Ir-based water-oxidation catalysts (WOCs) that can be activated either chemically or electrochemically.[5] Through collaborative theoretical and experimental efforts, the solution structures of Ir-pyalk WOCs have been determined.[6] Recent efforts have focused on developing WOCs based on earth-abundant metal centers, including manganese and copper.[7] However, the underlying reaction mechanisms of these new catalysts have yet to be established. In fact, little is known about the mechanism of electrocatalytic water oxidation by copper complexes despite the first molecular Cu WOC being reported in 2012.[8]

Three commonly proposed water-oxidation mechanisms for transition metal catalysts include water-nucleophilic attack (WNA) on a metal oxyl-radical species,[9,10] the interaction of two radical M−O• groups,[11] and redox isomerization.[12] Another possible mechanism, involving direct coupling to oxo bridges, was proposed by Siegbahn and co-workers for water oxidation in the Mn cluster of the oxygen-evolving complex of Photosystem II,[13] in synthetic Mn catalysts,[14] and in a dinuclear copper complex.[15] Additionally, hydroperoxo intermediates have also been reported by Maseras, Llobet, and co-workers in what is termed "single electron transfer (ET)/WNA".[16,17] Here, we explore the mechanism of the $Cu(pyalk)_2$ catalyst.

A recent study of dimeric copper WOCs has suggested that a dinuclear WNA or a redox-isomerization pathway may play a major role in copper-based electrocatalytic water oxidation.[12] Many copper WOCs have been shown to have first-order kinetics in copper over a wide concentration range, suggesting that a mononuclear pathway may be viable.[8] Such a pathway could occur through a Cu(III)-oxyl radical intermediate, rather than a Cu(IV)-oxo intermediate, consistent with the "oxo wall" concept (no tetragonal terminal oxo species have been isolated for any transition metal from group 9 onward).[18] Such species have been suggested[19] but never observed experimentally.

In this paper, we focus on elucidating the mechanism of the recently reported complex $Cu(pyalk)_2$ (**1**), found to be an active and robust electrocatalyst for water oxidation under basic conditions. We previously found that the catalyst has a TOF of 0.7 s^{-1}, at pH = 12.5, shows a first-order dependence on copper, and remains active for over 30 catalytic turnovers with minimal degradation.[7] However, neither the active form of the catalyst nor the catalytic mechanism could be resolved. In this work, we find that the catalyst is active only in the *cis* isomer, **2** (Chart 1). Our proposed mechanism involves proton-coupled electron transfer (PCET) based on a WNA onto a terminal oxyl radical species.

In this work, we investigate the catalytically active isomeric form and propose a plausible mechanism for a mononuclear

Received: June 25, 2018
Revised: July 16, 2018
Published: July 18, 2018

DOI: 10.1021/acscatal.8b02466
ACS Catal. 2018, 8, 7952−7960

Chart 1. Structure of the Proposed Active Form *cis*-$Cu^{II}(pyalk)_2$, (2)

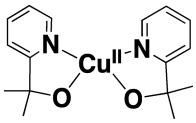

catalyst. The resulting mechanism accounts for the multiple oxidation state transitions that are required for water oxidation, offering fundamental insights valuable for development of earth-abundant WOCs.

THEORETICAL METHODS

Calculations were based on unrestricted density functional theory (DFT) using the functional ωB97X-D,[20,21] which includes dispersion interactions, as implemented in Gaussian 09, revision D.01.[22] Comparisons to calculations based on B3LYP[23] are included in the Supporting Information (SI). The ωB97X-D functional has been found to be quite useful for describing open-shell transition metal systems,[24] water clusters,[25] and hydrogen bonds.[26] The basis set used for geometry optimization, normal-mode analysis (and calculations of free energy corrections[27]), and time-dependent DFT (TDDFT) calculations included the double-ζ basis set def2-SVP[28] for all elements but O, which was treated with 6-31+G(d,p),[29,30] for the negative charges that reside on the anionic pyalk ligands, in particular, as recommended in the literature.[31,32] Single-point energy calculations of the optimized structures and wave function stability checks (for the minima)[33,34] were based on the triple-ζ basis set 6-311+G-(2df,p) for all atoms.[29,35−40] Calculations without the diffuse functions (def2-SVP for all atoms for the optimization and frequency calculations and def2-TZVP for all atoms in the single-point calculations) were done as a test, as discussed in section S9.

The Cu(II) and Cu(III)-oxyl radical species are open-shell doublets, with the former having the spin residing on the Cu and the latter having the spin residing on oxyl. Nevertheless, they do not to require corrections for spin contamination (SI, section S2). Table S2 gives the spin densities used to confirm the oxidation states of various radical species. We tested the possibility of a high-spin Cu(III) antiferromagnetically coupled to the oxyl radical and found that this configuration instead optimized to one with a Cu(II) and a pyalk O having spin densities of 0.66 and 0.84, respectively, antiferromagnetically coupled to the oxyl radical with a spin density of −0.88. Because it was more energetically costly by 4.6 kcal/mol and suffered from significant spin contamination, it was not considered further. Additionally, we tested other possible spin states for each species, as indicated in Table S3, which were all found to be higher in energy.

Calculations of imaginary frequencies and intrinsic reaction coordinates (IRCs) (using local quadratic approximations (LQAs)) were used to confirm the identity of the transition states.[41,42] These are given in the SI in section S5. Barrier heights are computed from the difference in free energies of the transition state and the minimum immediately before. The activation free energy for the overall reaction is taken as the activation free energy for WNA (step V) as its transition state is the highest point on the computed potential energy surface and the minimum preceding it is the lowest point, considering the potentials applied, as recommend in the literature.[43]

Theoretical UV−vis spectra were generated using 30 singlet states[44−50] and a Gaussian broadening factor with a full width at half-maximum (fwhm) of 4839.33 cm^{-1} (0.6 eV) chosen for best comparison to experiment. The intensities of the theoretical spectra were scaled consistently. The integration grid for the DFT multielectron integrals was "ultrafine", a pruned grid of 99 radial shells and 590 angular points for each shell. Structures were optimized to the rigorous "tight" criteria with a maximum step size of 0.000015 au, root-mean-square (RMS) step size of 0.000010 au, maximum force of 0.000060 au, and RMS force threshold of 0.000040 au.

Geometry optimizations of structures were undertaken within the dielectric continuum model, using the SMD[51−54] solvation model of water with a dielectric constant of 78.3553,[22] except when comparing to crystal structures, in which case, the gas-phase structure was used. Concentration effects were taken into account as described in the SI (section S3). The literature value for the solvation energy of a proton is the sum of −264.0 and the −1.9 kcal/mol concentration correction from 1 atm to 1 M.[55,56] Potentials for oxidation were calculated and referred to the calculation for the novel compound **9** in the Cu^{II} and Cu^{III} oxidation states, using the experimental value vs NHE (1.07 V vs NHE)[7] as recommended in our previous work.[57] The absolute potential approach of using 4.281 V[14,58−60] yields similar results as shown in section S8 of the SI, though it performs worse for the reference compound **9**, which has no isomeric ambiguities; therefore, we do not use it. The potentials of PCET steps are corrected for a pH of 13 using the Nernst equation.

RESULTS AND DISCUSSION

1. Validation of Model Chemistry. Table 1 shows that the minimum-energy structure obtained at the DFT ωB97X-D/(def2-SVP,6-31+G(d,p)) level in the gas phase reproduces the crystal structure of **1**. Figure 1 shows that, with this level of theory, either isomer or a combination of both is consistent with the UV−vis absorption features in water.

2. Exclusion of Other Mechanisms. In our previous work, we studied the dependence of the peak catalytic current over a wide range of catalyst concentrations and observed no deviations from linearity, even at low catalyst concentrations. This first-order behavior is consistent with a mononuclear

Table 1. Average Theoretical (theor.) Bond Lengths, Bond Angles, and Dihedrals of 1[a] in the Gas Phase As Compared to Experimental Values (expt)[b]

	Cu−N (Å)	Cu−O (Å)	N−O−Cu (intra) (deg)	N−O−Cu (inter) (deg)	N−C−C−O (deg)
theor.	1.99	1.89	83.7	96.3	0
expt.	1.972(2)	1.883(1)	84.04(5)	95.96	−6.528

[a]Without hydrogen-bonding waters. [b]See ref 7. intra indicates a bond angle defined within one pyalk ligand, whereas inter indicates a bond angle defined spanning two pyalk ligands.

DOI: 10.1021/acscatal.8b02466
ACS Catal. 2018, 8, 7952−7960

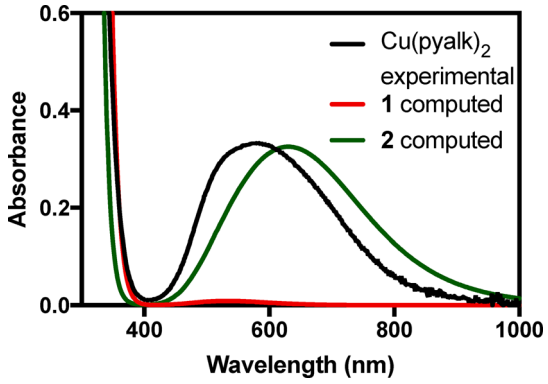

Figure 1. Computed UV−vis spectra for *trans* (**1**) and *cis* (**2**) as compared to the experimental spectrum of a 2 mM sample in water.[7]

mechanism.[7] We, therefore, did not investigate dinuclear mechanisms such as redox isomerization[12] or μ-oxo coupling,[15] which have been proposed for preorganized dimeric catalysts. A reaction between two oxyl radicals is also unlikely as these species are presumably short-lived and would be expected to undergo mononuclear rather than dinuclear reactions. There is experimental and theoretical evidence to support mononuclear Cu sites in lytic polysaccharide monooxygenase[61] and methane monooxygenase.[62] Additionally, the stability of the ligand under these oxidizing conditions has been confirmed experimentally in our previous work using cyclic voltammetry (CV).[7] The proposed redox-inactivity of the pyalk ligand is consistent with the deep-lying ligand HOMO found theoretically (Figure S9). Thus, we could rule out mechanisms involving a redox-active ligand, such as single ET/WNA.[16,17] Therefore, we investigated WNA as the most plausible mechanism and tested it against both theory and experiment; the good agreement that we found validates our approach.

3. Water-Nucleophilic Attack Mechanism. Scheme 1 shows the mechanism appropriate for basic solutions predicted by DFT calculations, which includes bulk solvation from the dielectric continuum model as well as direct solvation by two hydrogen-bonded waters to the pyalk oxygen atoms.

Step **I** (Scheme 1) involves the conversion of *trans*-$Cu^{II}(pyalk)_2$ (**1**) into the *cis* form (**2**), which involves a ΔG of about 2.8 kcal/mol. Therefore, while there is more *trans*-$Cu(pyalk)_2$ in solution, there is still a catalytically relevant amount of *cis* form available. The conformational changes induced by the **1** → **2** conversion are shown in Figure 2.

Step **II** (Scheme 1) involves oxidation of Cu^{II} to Cu^{III} in the *cis* form, which includes a first-coordination-sphere bond shortening of ∼0.11 Å. The experimental potential for this quasireversible conversion is shown to be 1.3 V vs NHE.[7] The calculated reversible potentials for oxidation of the *cis* and *trans* forms are 1.0 and 1.2 V vs NHE, respectively. The calculated values for both isomers differ systematically from experiment, likely due to the lack of reversibility in the experimental

Scheme 1. Mechanism of Water Oxidation Catalyzed by the Complex $Cu^{II}(pyalk)_2$, (1)[a]

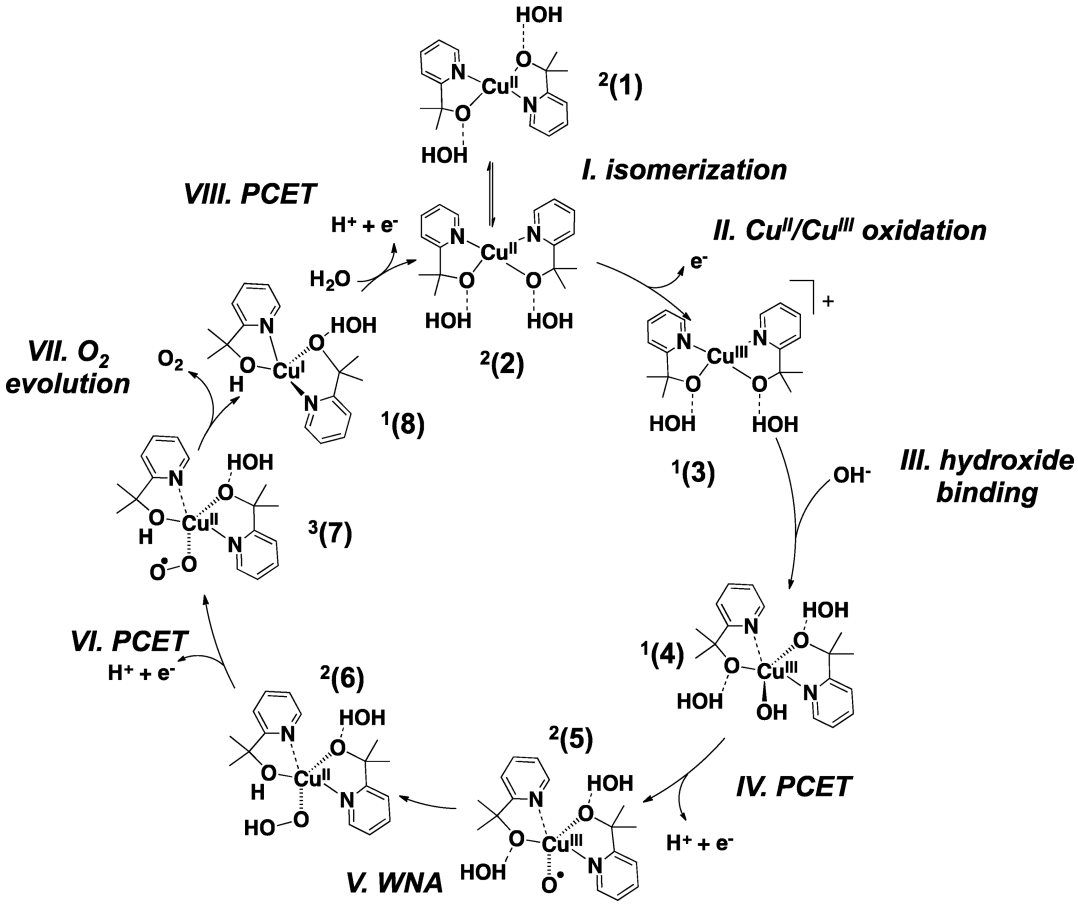

[a]The superscripted number indicates the multiplicity.

DOI: 10.1021/acscatal.8b02466
ACS Catal. 2018, 8, 7952−7960

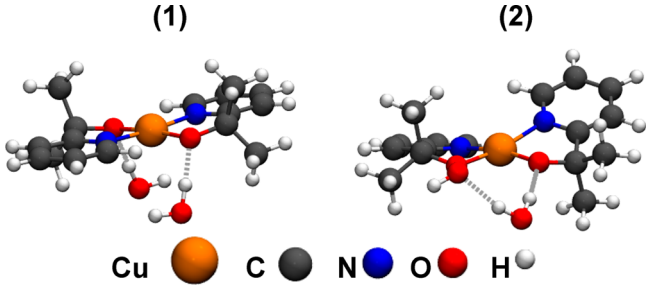

Figure 2. DFT optimized structures of **1** and **2**. The color code is indicated at the bottom of the figure. Hydrogen bonds are indicated by dashed lines.

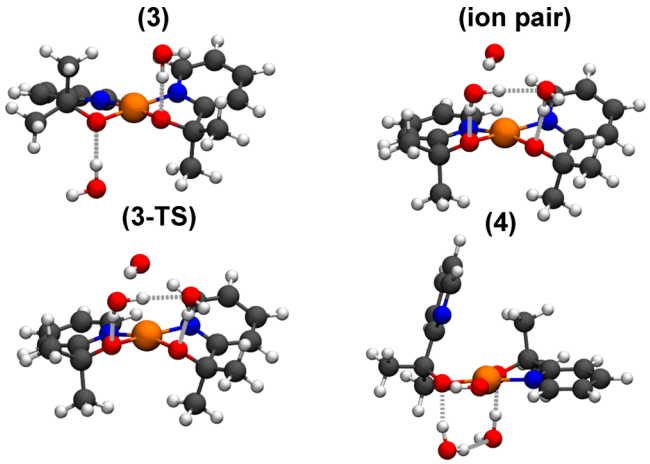

Figure 3. DFT optimized structures of intermediates **3** and **4** as well as the ion pair and transition states.

measurement and the difficulty of modeling the aqueous environment. Intermediate **3** is illustrated in Figure 3.

Step **III** (Scheme 1) involves binding of hydroxide to form a cationic five-coordinate Cu^{III} species, **4** (Figure 3), because water deprotonates when attached to Cu^{III}. The free energy was computed in two parts, including formation of the ion pair and the actual nucleophilic attack via **3-TS**, as shown in Figure 3. The free energy change necessary to form the ion pair is ΔG = 5.0 kcal/mol, dominated by the entropic term (ΔS = −23.9 cal mol^{-1} K^{-1}), though this energy may be overestimated as ion pairs often form spontaneously in solution. From the ion pair, the free energy change for attachment to Cu is ΔG = −15.8 kcal/mol, leading to an overall free energy change of ΔG = −10.8 kcal/mol. The barrier for the nucleophilic attack is 1.0 kcal/mol. Therefore, the barrier for the overall step is $\Delta G^{\ddagger}_{total} = \Delta G_{ion\ pair} + \Delta G^{\ddagger}$ = 5.0 + 1.0 kcal/mol = 6.0 kcal/mol.

Step **IV** of the cycle involves formation of the oxyl radical, **5**, likely through PCET at the expense of 1.3 V vs NHE. The oxidation affects the hydroxyl ligand to form an oxyl radical, rather than forming a high-energy Cu^{IV} species, for which we could not even identify a stable structure as expected from the "oxo wall" principle. The oxyl-radical intermediate has the structure given in Figure 4 and a spin density of 0.998 on the oxyl oxygen atom while copper has essentially 0 spin density (Table S2). The presence of this second oxidation step cannot be ruled out experimentally as estimating the area under the CV trace is complicated by the fact that the reagent (OH^-) is part of the solvent. Stepwise proton transfer (PT) followed by ET and the reverse were ruled out by evaluating each step

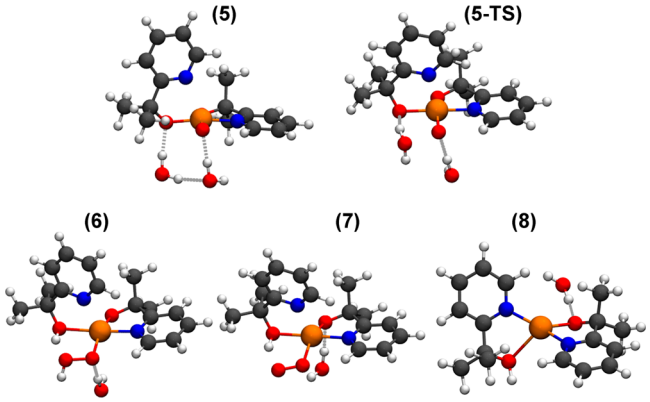

Figure 4. DFT optimized structures of intermediates **5**−**8** as well as the transition state **5-TS**.

separately and finding that the pK_a of the initial deprotonation step or the potential of the initial oxidation step would be inaccessible under our conditions, as shown in section S6 of the SI.

Step **V** (Scheme 1) is the nucleophilic attack water on the oxyl radical with a synchronous PT to the nearby alkoxide oxygen of the pyalk ligand (Figure 4). The transition state for that process, **5-TS**, and the resulting peroxy intermediate **6** are illustrated in Figure 4, while the mechanism is illustrated in Scheme 2.

Scheme 2. WNA Mechanism onto the Oxyl Radical of 5 to Form 6 upon PT to the pyalk Ligand (as shown in Scheme 1)

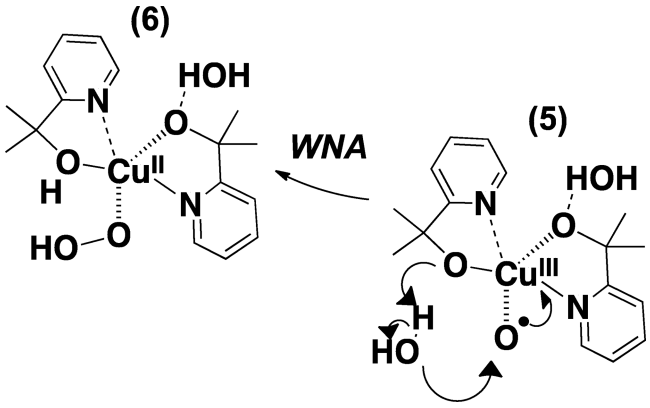

The net free energy change is ΔG = −20.4 kcal/mol, and the activation free energy $\Delta G^{\ddagger}$ is 19.3 kcal/mol. To compare to the experimental TOF = 0.7 s^{-1},[7] we used the Eyring equation of transition state theory

$$k = \frac{k_b T}{h} \exp\left(\frac{-\Delta G^{\ddagger}}{RT}\right)$$

which predicts an experimental barrier of 17.6 kcal/mol. Here, the alkoxide O of the pyalk acts to weaken the Cu−O bond via the *trans* effect, consistent with the finding that the *cis* isomer **2** is the active species, as the other pyalk O must be *cis* to both other O atoms (it is not stable as an axial ligand). Despite our best efforts, we could not locate the equivalent transition state of **5-TS** with the N *trans* to the oxyl radical, though the mechanism should, in principle, be much the same. Instead, we

DOI: 10.1021/acscatal.8b02466
ACS Catal. 2018, 8, 7952−7960

found that this configuration led to an unproductive pathway where the pyalk O attacked the radical instead and the resulting barrier for WNA would be too high (section S10).

Step **VI** (Scheme 1) involves another PCET oxidation on the terminal hydroxyl group, forming a triplet diradical with one spin shared by the two oxygens of the peroxyl group (**7** as shown in Figure 4), aligned parallel to the spin of Cu^{II}. The potential for this PCET is only −0.5 V vs NHE, making it easily accessible.

Step **VII** involves triplet oxygen evolution through the mechanism illustrated in Scheme 3, with a modest ΔG = 4.0 kcal/mol, forming a tetrahedral Cu^{I} with one of the pyalk groups still protonated.

Scheme 3. Mechanism of O_2 Evolution to Form 8 According to the Reaction Mechanism of Scheme 1[a]

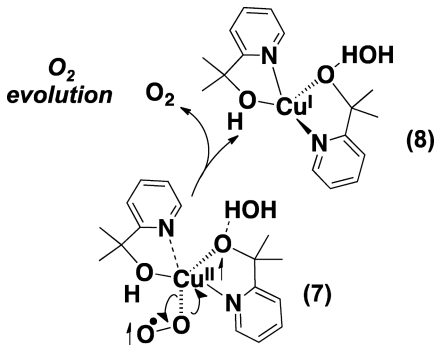

[a]Spin alignment is indicated for the terminal oxyl and Cu center.

Step **VIII** completes the cycle with another PCET that regenerates the Cu^{II} complex in the *cis* form, **2**. The subsequent oxidation is quite facile, with a potential of −1.1 V vs NHE. Figure 5 shows the potential surface for the entire mechanism under the conditions of zero bias potential and an operating potential of 1.3 V vs NHE.

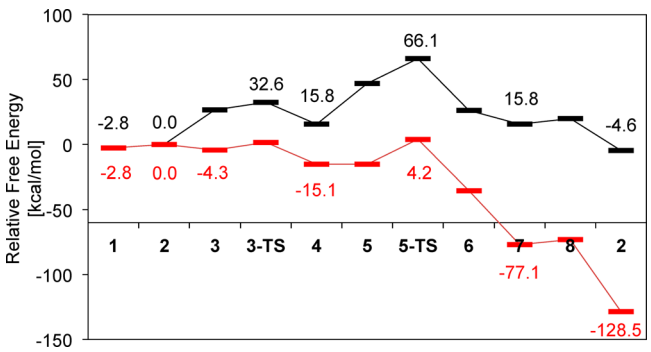

Figure 5. Free potential energy surface for the water-oxidation reaction catalyzed by (**2**) under 0 bias (black, U = 0 V vs NHE) and operating conditions defined as U = 1.3 V vs NHE (red).

An equivalent mechanism was found with the B3LYP functional (shown in Figures S5 and S6) with the transition state **5-TS** becoming just a PT from the water to pyalk. Then two additional structures, **A**, a minimum, and **A-TS**, a transition state, for the O−O bond formation (highest point on the surface) were found. The mechanism still involves a WNA though a predicted barrier of 16.2 kcal/mol (TOF = 8.03 s^{-1}).

4. Experimental Corroboration. The mechanism described in Scheme 1 implies that a pyridine−Cu bond is lengthened and ultimately dissociates from the Cu center in intermediates **4**−**7**, opening up a binding site for substrate water. Therefore, a complex with a similar ligand scaffold but without pyridine flexibility should, in principle, be unable to perform catalysis. To test this hypothesis, complex **9** (Figure 6) was synthesized.[63]

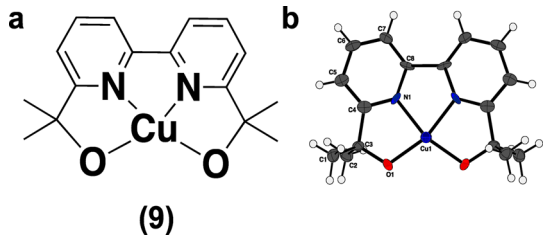

Figure 6. (a) Structure of complex **9** Cu^{II}(bipydipyalk)$_2$ and (b) X-ray crystallographic model. Only the asymmetric unit is labeled. Symmetry-equivalent atom positions are generated by the operator (1/2) − x, (1/2) − y, z. Thermal ellipsoids are shown at the 50% probability level (SI, section S1).

Like Cu(pyalk)$_2$, **9** has two alkoxo and two pyridyl groups, but the rigid, tetradentate ligand scaffold does not allow for flexibility of either pyridine and would have difficulty supporting the tetrahedral Cu^{I} intermediate **8**. Under the electrocatalytic conditions used for water oxidation by Cu(pyalk)$_2$, **9** was found not to be competent for water-oxidation catalysis, as shown in Figure 7, thus supporting the catalytic mechanism of Scheme 1.

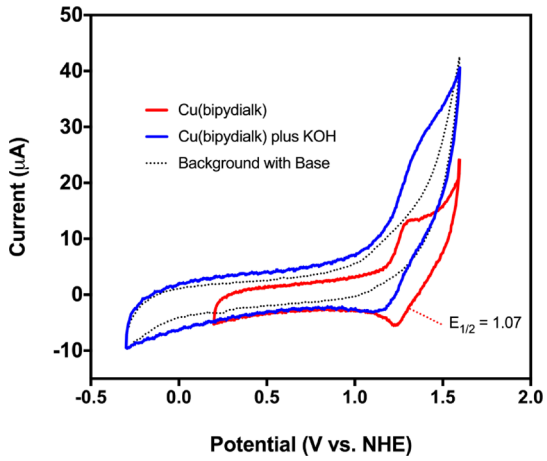

Figure 7. CV of **9** in the absence and presence of KOH. Under basic conditions, no enhancement of current above background levels is observed.

Foot-of-the-wave analysis of the catalytic current was used to provide mechanistic information on the chemical step following ET.[64] For a WNA mechanism in a homogeneous electrocatalytic system, the foot-of-the-wave region can be modeled as follows

$$\frac{i}{i_p} = \frac{4 \times 2.24\sqrt{\frac{RT}{F\nu}k_1}}{1 + e^{F(E^0 - E)/RT}}$$

DOI: 10.1021/acscatal.8b02466
ACS Catal. 2018, 8, 7952−7960

where i is the current of the catalytic process, i_p is the peak current intensity of a one-electron noncatalytic process, ν is the scan rate, E is applied potential, E^0 is the standard potential of the first ET step, R is the gas constant, T is temperature, F is Faraday's constant, and k_1 is the pseudo-first-order rate constant associated with the chemical step following the first ET.

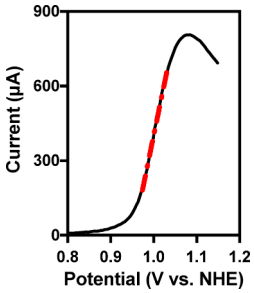

Figure 8. Linear sweep voltammogram of 2 mM **1** in 0.1 M KNO_3 adjusted to pH 13 with 0.1 M KOH (black). The region used for foot-of-the-wave calculations is shown in red.

For **1**, the linear fit of the foot-of-the-wave region leads to a rate of about 3×10^7 s^{-1} (Figures 8 and S4), while the barrier for the hydroxide nucleophilic attack was estimated to be 5.9 kcal/mol (2.8×10^8 s^{-1}) with the ωB97X-D functional and 9.6 kcal/mol (5.6×10^5 s^{-1}) with B3LYP; therefore, the experimental estimation is within the range of values predicted by DFT when combined with transition state theory.

The H/D kinetic isotope effect (KIE) was measured by comparing the cyclic voltammograms of **1** in 0.01 M NaOH and 0.01 M NaOD solution (Figure 9), respectively, both solutions with 0.1 M KNO_3 as the electrolyte.

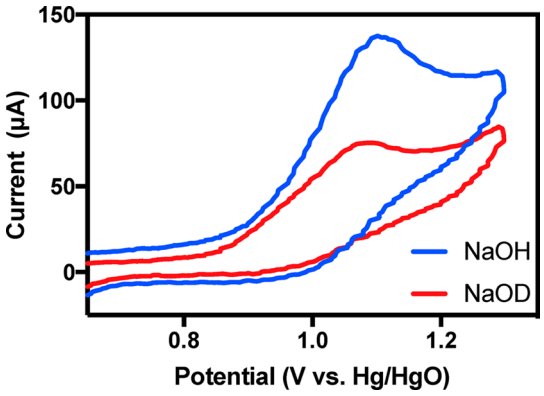

Figure 9. Cyclic voltammograms of 0.5 mM **1** with [NaOH] = [NaOD] = 0.01 M. CVs were taken with a boron-doped diamond working electrode, Pt wire counter electrode, and Hg/HgO reference electrode at a scan rate of 100 mV/s.

The H/D KIE was obtained as follows

$$\mathrm{KIE} = \frac{k_{H_2O}}{k_{D_2O}} = \left(\frac{i_{H_2O}}{i_{D_2O}}\right)^2 = \left(\frac{nFA[C]\sqrt{Dk_{H_2O}}}{nFA[C]\sqrt{Dk_{D_2O}}}\right)^2 \quad (1)$$

where i = current, n = number of electrons in the catalytic process, F = Faraday's constant, A = surface area of the electrode, [C] = catalyst concentration, D = diffusion coefficient of the catalyst, and k = pseudo-first-order rate constant. The resulting experimental H/D KIE was found to be 3.4, consistent with proton involvement in the rate-determining step as in the proposed mechanism. The estimated KIE is similar to those found for several other mononuclear copper WOCs but is in stark contrast with those reported for dinuclear catalysts, as shown in Table 2.

Table 2. Literature Values for H/D KIEs for Molecular Copper WOCs

Compound	Nuclearity of Cu	KIE	Ref.
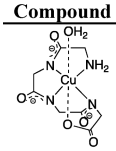	Mono	2.0	65
	Mono	2.1	66
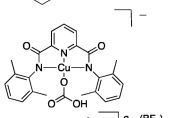	Mono	1.81	67
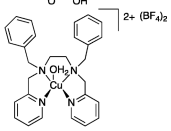	Mono	2.0	68
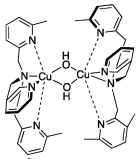	Di	20	12
Cu^{2+}	Mono	1.01	69

For comparison, we computed the KIE with exchangeable polar hydrogen atoms swapped with deuterium atoms. We focused on the rate-determining step **5** → **5-TS** because chemical steps do not immediately precede it. The resulting KIE was evaluated as in our previous studies,[10] using transition state theory, as shown in eq 2.[70,71]

$$\mathrm{KIE} = \frac{k_{H_2O}}{k_{D_2O}} = \left(\frac{e^{-(-G_{R(H_2O)}+G_{TS(H_2O)})/RT}}{e^{-(-G_{R(D_2O)}+G_{TS(D_2O)})/RT}}\right) = e^{-(G_{R(D_2O)}+G_{TS(H_2O)}-G_{R(H_2O)}-G_{TS(D_2O)})/RT} \quad (2)$$

The calculated KIE was 3.7, which is in excellent agreement with the experimental value (3.4), further supporting the proposed WNA mechanism. For comparison, hydroxide binding to Cu^{III} exhibits a KIE of only 1.1, confirming that hydroxide binding is not rate-limiting.

Further work to corroborate the proposed mechanism could involve immobilization of catalysts on electrode surfaces and measurements of other catalytic and electrochemical parameters, including $^{16}O/^{18}O$ KIEs under electrocatalytic conditions.

■ CONCLUSIONS

We have shown that the $Cu^{II}(pyalk)_2$ complex catalyzes water oxidation through a WNA onto an oxyl radical, formed upon substrate water binding and oxidation by PCET. Remarkably, the pyalk ligand has the ability to remain bound even with a labile pyridine group that opens a coordination site for substrate water binding, enabling robust functionality of a labile first-row transition metal catalyst. The proposed mechanism is supported by measurements of the KIE and

DOI: 10.1021/acscatal.8b02466
ACS Catal. 2018, 8, 7952−7960

foot-of-the-wave electrochemical analysis. The resulting insights are particularly valuable for ligand design and development of even more efficient WOCs based on earth-abundant transition metal complexes.

■ ASSOCIATED CONTENT

Supporting Information

The Supporting Information is available free of charge on the ACS Publications website at DOI: 10.1021/acscatal.8b02466.

Experimental methods, spin contamination check including spin densities, concentration corrections, additional references and coordinates of structurally optimized molecules (PDF)

Structures of the molecules studied (ZIP)

■ AUTHOR INFORMATION

Corresponding Authors

*E-mail: gary.brudvig@yale.edu. Phone: (203) 432-5202. Fax: (203) 432-6144 (G.W.B.).

*E-mail: robert.crabtree@yale.edu. Phone: (203) 432-3925. Fax: (203) 432-6144 (R.H.C.).

*E-mail victor.batista@yale.edu. Phone: (203) 432-6672. Fax: (203) 432-6144 (V.S.B.).

ORCID

Benjamin Rudshteyn: 0000-0002-9511-6780

Gary W. Brudvig: 0000-0002-7040-1892

Robert H. Crabtree: 0000-0002-6639-8707

Victor S. Batista: 0000-0002-3262-1237

Notes

The authors declare no competing financial interest.

■ ACKNOWLEDGMENTS

V.S.B., R.H.C., and G.W.B. acknowledge financial support as a part of the Argonne−Northwestern Solar Energy Research (ANSER) Center of the federally funded Energy Frontier Research Center (Award Number DE-SC0001059). V.S.B. acknowledges high-performance computing time from NERSC, from DOD Copper, and from the Center for Research Computing at Yale University. This work used the Extreme Science and Engineering Discovery Environment (XSEDE), which is supported by National Science Foundation Grant Number ACI-1053575. B.R. and K.J.F. gratefully acknowledge support from the NSF Graduate Research Fellowship under Grant No. DGE-1122492. B.R. thanks the Energy Sciences Institute members, particularly Dr. Svante Hedström, Dr. Atanu Acharya, and Dr. Uriel Morzan, for helpful comments.

■ REFERENCES

(1) Young, K. J.; Martini, L. A.; Milot, R. L.; Snoeberger, R. C.; Batista, V. S.; Schmuttenmaer, C. A.; Crabtree, R. H.; Brudvig, G. W. Light-Driven Water Oxidation for Solar Fuels. *Coord. Chem. Rev.* **2012**, *256*, 2503−2520.

(2) Blakemore, J. D.; Crabtree, R. H.; Brudvig, G. W. Molecular Catalysts for Water Oxidation. *Chem. Rev.* **2015**, *115*, 12974−13005.

(3) Thomsen, J. M.; Huang, D. L.; Crabtree, R. H.; Brudvig, G. W. Iridium-Based Complexes for Water Oxidation. *Dalton Trans.* **2015**, *44*, 12452−12472.

(4) Garrido-Barros, P.; Gimbert-Suriñach, C.; Matheu, R.; Sala, X.; Llobet, A. How to Make an Efficient and Robust Molecular Catalyst for Water Oxidation. *Chem. Soc. Rev.* **2017**, *46*, 6088−6098.

(5) Michaelos, T. K.; Shopov, D. Y.; Sinha, S. B.; Sharninghausen, L. S.; Fisher, K. J.; Lant, H. M. C.; Crabtree, R. H.; Brudvig, G. W. A Pyridine Alkoxide Chelate Ligand That Promotes Both Unusually High Oxidation States and Water-Oxidation Catalysis. *Acc. Chem. Res.* **2017**, *50*, 952−959.

(6) Yang, K. R.; Matula, A. J.; Kwon, G.; Hong, J.; Sheehan, S. W.; Thomsen, J. M.; Brudvig, G. W.; Crabtree, R. H.; Tiede, D. M.; Chen, L. X.; Batista, V. S. Solution Structures of Highly Active Molecular Ir Water-Oxidation Catalysts from Density Functional Theory Combined with High-Energy X-ray Scattering and EXAFS Spectroscopy. *J. Am. Chem. Soc.* **2016**, *138*, 5511−5514.

(7) Fisher, K. J.; Materna, K. L.; Mercado, B. Q.; Crabtree, R. H.; Brudvig, G. W. Electrocatalytic Water Oxidation by a Copper(II) Complex of an Oxidation-Resistant Ligand. *ACS Catal.* **2017**, *7*, 3384−3387.

(8) Barnett, S. M.; Goldberg, K. I.; Mayer, J. M. A Soluble Copper−Bipyridine Water-Oxidation Electrocatalyst. *Nat. Chem.* **2012**, *4*, 498−502.

(9) Hughes, T. F.; Friesner, R. A. Systematic Investigation of the Catalytic Cycle of a Single Site Ruthenium Oxygen Evolving Complex Using Density Functional Theory. *J. Phys. Chem. B* **2011**, *115*, 9280−9289.

(10) Khan, S.; Yang, K. R.; Ertem, M. Z.; Batista, V. S.; Brudvig, G. W. Mechanism of Manganese-Catalyzed Oxygen Evolution from Experimental and Theoretical Analyses of ^{18}O Kinetic Isotope Effects. *ACS Catal.* **2015**, *5*, 7104−7113.

(11) Francàs, L.; Sala, X.; Benet-Buchholz, J.; Escriche, L.; Llobet, A. A Ru-Hbpp-Based Water-Oxidation Catalyst Anchored on Rutile TiO_2. *ChemSusChem* **2009**, *2*, 321−329.

(12) Koepke, S. J.; Light, K. M.; VanNatta, P. E.; Wiley, K. M.; Kieber-Emmons, M. T. Electrocatalytic Water Oxidation by a Homogeneous Copper Catalyst Disfavors Single-Site Mechanisms. *J. Am. Chem. Soc.* **2017**, *139*, 8586−8600.

(13) Siegbahn, P. E. M. Nucleophilic Water Attack Is Not a Possible Mechanism for O−O Bond Formation in Photosystem II. *Proc. Natl. Acad. Sci. U. S. A.* **2017**, *114*, 4966−4968.

(14) Liao, R.-Z.; Siegbahn, P. E. M. Quantum Chemical Modeling of Homogeneous Water Oxidation Catalysis. *ChemSusChem* **2017**, *10*, 4236−4263.

(15) Su, X. J.; Gao, M.; Jiao, L.; Liao, R. Z.; Siegbahn, P. E. M.; Cheng, J. P.; Zhang, M. T. Electrocatalytic Water Oxidation by a Dinuclear Copper Complex in a Neutral Aqueous Solution. *Angew. Chem., Int. Ed.* **2015**, *54*, 4909−4914.

(16) Garrido-Barros, P.; Funes-Ardoiz, I.; Drouet, S.; Benet-Buchholz, J.; Maseras, F.; Llobet, A. Redox Non-Innocent Ligand Controls Water Oxidation Overpotential in a New Family of Mononuclear Cu-Based Efficient Catalysts. *J. Am. Chem. Soc.* **2015**, *137*, 6758−6761.

(17) Funes-Ardoiz, I.; Garrido-Barros, P.; Llobet, A.; Maseras, F. Single Electron Transfer Steps in Water Oxidation Catalysis. Redefining the Mechanistic Scenario. *ACS Catal.* **2017**, *7*, 1712−1719.

(18) Winkler, J. R.; Gray, H. B. *Molecular Electronic Structures of Transition Metal Complexes I*; Springer, 2011; pp 17−28.

(19) Zhang, M.-T.; Chen, Z.; Kang, P.; Meyer, T. J. Electrocatalytic Water Oxidation with a Copper(II) Polypeptide Complex. *J. Am. Chem. Soc.* **2013**, *135*, 2048−2051.

(20) Chai, J.-D.; Head-Gordon, M. Long-Range Corrected Hybrid Density Functionals with Damped Atom-Atom Dispersion Corrections. *Phys. Chem. Chem. Phys.* **2008**, *10*, 6615−6620.

(21) Chai, J.-D.; Head-Gordon, M. Systematic Optimization of Long-Range Corrected Hybrid Density Functionals. *J. Chem. Phys.* **2008**, *128*, 084106.

(22) Frisch, M. J.; Trucks, G. W.; Schlegel, H. B.; Scuseria, G. E.; Robb, M. A.; Cheeseman, J. R.; Scalmani, G.; Barone, V.; Mennucci, B.; Petersson, G. A.; Nakatsuji, H.; Caricato, M.; Li, X.; Hratchian, H. P.; Izmaylov, A. F.; Bloino, J.; Zheng, G.; Sonnenberg, J. L.; Hada, M.; Ehara, M.; Toyota, K.; Fukuda, R.; Hasegawa, J.; Ishida, M.; Nakajima, T.; Honda, Y.; Kitao, O.; Nakai, H.; Vreven, T.;

DOI: 10.1021/acscatal.8b02466
ACS Catal. 2018, 8, 7952−7960

Montgomery, J. A., Jr.; Peralta, J. E.; Ogliaro, F.; Bearpark, M.; Heyd, J. J.; Brothers, E.; Kudin, K. N.; Staroverov, V. N.; Kobayashi, R.; Normand, J.; Raghavachari, K.; Rendell, A.; Burant, J. C.; Iyengar, S. S.; Tomasi, J.; Cossi, M.; Rega, N.; Millam, N. J.; Klene, M.; Knox, J. E.; Cross, J. B.; Bakken, V.; Adamo, C.; Jaramillo, J.; Gomperts, R.; Stratmann, R. E.; Yazyev, O.; Austin, A. J.; Cammi, R.; Pomelli, C.; Ochterski, J. W.; Martin, R. L.; Morokuma, K.; Zakrzewski, V. G.; Voth, G. A.; Salvador, P.; Dannenberg, J. J.; Dapprich, S.; Daniels, A. D.; Farkas, Ö.; Foresman, J. B.; Ortiz, J. V.; Cioslowski, J.; Fox, D. J. *Gaussian 09*, revision D.01; Gaussian, Inc.: Wallingford, CT, 2009.

(23) Becke, A. D. Density-Functional Thermochemistry. III. The Role of Exact Exchange. *J. Chem. Phys.* **1993**, *98*, 5648−5652.

(24) Luo, S.; Averkiev, B.; Yang, K. R.; Xu, X.; Truhlar, D. G. Density Functional Theory of Open-Shell Systems. The 3d-Series Transition-Metal Atoms and Their Cations. *J. Chem. Theory Comput.* **2014**, *10*, 102−121.

(25) Howard, J. C.; Enyard, J. D.; Tschumper, G. S. Assessing the Accuracy of Some Popular DFT Methods for Computing Harmonic Vibrational Frequencies of Water Clusters. *J. Chem. Phys.* **2015**, *143*, 214103.

(26) Thanthiriwatte, K. S.; Hohenstein, E. G.; Burns, L. A.; Sherrill, C. D. Assessment of the Performance of DFT and DFT-D Methods for Describing Distance Dependence of Hydrogen-Bonded Interactions. *J. Chem. Theory Comput.* **2011**, *7*, 88−96.

(27) Cramer, C. J. *Essentials of Computational Chemistry: Theories and Models*; John Wiley & Sons: West Sussex, England, 2004; pp 355−383.

(28) Weigend, F.; Ahlrichs, R. Balanced Basis Sets of Split Valence, Triple Zeta Valence and Quadruple Zeta Valence Quality for H to Rn: Design and Assessment of Accuracy. *Phys. Chem. Chem. Phys.* **2005**, *7*, 3297−3305.

(29) Clark, T.; Chandrasekhar, J.; Spitznagel, G. W.; Schleyer, P. V. R. Efficient Diffuse Function-Augmented Basis Sets for Anion Calculations. III. The 3-21+G Basis Set for First-Row Elements, Li−F. *J. Comput. Chem.* **1983**, *4*, 294−301.

(30) Hehre, W. J.; Ditchfield, R.; Pople, J. A. Self—Consistent Molecular Orbital Methods. XII. Further Extensions of Gaussian-Type Basis Sets for Use in Molecular Orbital Studies of Organic Molecules. *J. Chem. Phys.* **1972**, *56*, 2257−2261.

(31) Baik, M.-H.; Friesner, R. A. Computing Redox Potentials in Solution: Density Functional Theory as a Tool for Rational Design of Redox Agents. *J. Phys. Chem. A* **2002**, *106*, 7407−7412.

(32) Tsipis, A. C. DFT Flavor of Coordination Chemistry. *Coord. Chem. Rev.* **2014**, *272*, 1−29.

(33) Seeger, R.; Pople, J. A. Self-Consistent Molecular Orbital Methods. XVIII. Constraints and Stability in Hartree−Fock Theory. *J. Chem. Phys.* **1977**, *66*, 3045−3050.

(34) Bauernschmitt, R.; Ahlrichs, R. Stability Analysis for Solutions of the Closed Shell Kohn−Sham Equation. *J. Chem. Phys.* **1996**, *104*, 9047−9052.

(35) Wachters, A. J. H. Gaussian Basis Set for Molecular Wavefunctions Containing Third-Row Atoms. *J. Chem. Phys.* **1970**, *52*, 1033−1036.

(36) Hay, P. J. Gaussian Basis Sets for Molecular Calculations. The Representation of 3D Orbitals in Transition-Metal Atoms. *J. Chem. Phys.* **1977**, *66*, 4377−4384.

(37) Krishnan, R.; Binkley, J. S.; Seeger, R.; Pople, J. A. Self-Consistent Molecular Orbital Methods. XX. A Basis Set for Correlated Wave Functions. *J. Chem. Phys.* **1980**, *72*, 650−654.

(38) McLean, A.; Chandler, G. Contracted Gaussian Basis Sets for Molecular Calculations. I. Second Row Atoms, Z= 11−18. *J. Chem. Phys.* **1980**, *72*, 5639−5648.

(39) Frisch, M. J.; Pople, J. A.; Binkley, J. S. Self-Consistent Molecular Orbital Methods XXV. Supplementary Functions for Gaussian Basis Sets. *J. Chem. Phys.* **1984**, *80*, 3265−3269.

(40) Raghavachari, K.; Trucks, G. W. Highly Correlated Systems. Excitation Energies of First Row Transition Metals Sc−Cu. *J. Chem. Phys.* **1989**, *91*, 1062−1065.

(41) Page, M.; McIver, J. W., Jr On Evaluating the Reaction Path Hamiltonian. *J. Chem. Phys.* **1988**, *88*, 922−935.

(42) Page, M.; Doubleday, C.; McIver, J. W., Jr Following Steepest Descent Reaction Paths. The Use of Higher Energy Derivatives with *ab initio* Electronic Structure Methods. *J. Chem. Phys.* **1990**, *93*, 5634−5642.

(43) Kozuch, S.; Shaik, S. How to Conceptualize Catalytic Cycles? The Energetic Span Model. *Acc. Chem. Res.* **2011**, *44*, 101−110.

(44) Bauernschmitt, R.; Ahlrichs, R. Treatment of Electronic Excitations Within the Adiabatic Approximation of Time Dependent Density Functional Theory. *Chem. Phys. Lett.* **1996**, *256*, 454−464.

(45) Casida, M. E.; Jamorski, C.; Casida, K. C.; Salahub, D. R. Molecular Excitation Energies to High-Lying Bound States from Time-Dependent Density-Functional Response Theory: Characterization and Correction of the Time-Dependent Local Density Approximation Ionization Threshold. *J. Chem. Phys.* **1998**, *108*, 4439−4449.

(46) Furche, F.; Ahlrichs, R. Adiabatic Time-Dependent Density Functional Methods for Excited State Properties. *J. Chem. Phys.* **2002**, *117*, 7433−7447.

(47) Scalmani, G.; Frisch, M. J.; Mennucci, B.; Tomasi, J.; Cammi, R.; Barone, V. Geometries and Properties of Excited States in the Gas Phase and in Solution: Theory and Application of a Time-Dependent Density Functional Theory Polarizable Continuum Model. *J. Chem. Phys.* **2006**, *124*, 094107.

(48) Stratmann, R. E.; Scuseria, G. E.; Frisch, M. J. An Efficient Implementation of Time-Dependent Density-Functional Theory for the Calculation of Excitation Energies of Large Molecules. *J. Chem. Phys.* **1998**, *109*, 8218−8224.

(49) Van Caillie, C.; Amos, R. D. Geometric Derivatives of Excitation Energies Using SCF and DFT. *Chem. Phys. Lett.* **1999**, *308*, 249−255.

(50) Van Caillie, C.; Amos, R. D. Geometric Derivatives of Density Functional Theory Excitation Energies Using Gradient-Corrected Functionals. *Chem. Phys. Lett.* **2000**, *317*, 159−164.

(51) Marenich, A. V.; Cramer, C. J.; Truhlar, D. G. Universal Solvation Model Based on Solute Electron Density and on a Continuum Model of the Solvent Defined by the Bulk Dielectric Constant and Atomic Surface Tensions. *J. Phys. Chem. B* **2009**, *113*, 6378−6396.

(52) Improta, R.; Barone, V.; Scalmani, G.; Frisch, M. J. A State-Specific Polarizable Continuum Model Time Dependent Density Functional Theory Method for Excited State Calculations in Solution. *J. Chem. Phys.* **2006**, *125*, 054103.

(53) Improta, R.; Scalmani, G.; Frisch, M. J.; Barone, V. Toward Effective and Reliable Fluorescence Energies in Solution by a New State Specific Polarizable Continuum Model Time Dependent Density Functional Theory Approach. *J. Chem. Phys.* **2007**, *127*, 074504.

(54) Scalmani, G.; Frisch, M. J. Continuous Surface Charge Polarizable Continuum Models of Solvation. I. General Formalism. *J. Chem. Phys.* **2010**, *132*, 114110.

(55) Tissandier, M. D.; Cowen, K. A.; Feng, W. Y.; Gundlach, E.; Cohen, M. H.; Earhart, A. D.; Coe, J. V.; Tuttle, T. R. The Proton's Absolute Aqueous Enthalpy and Gibbs Free Energy of Solvation from Cluster-Ion Solvation Data. *J. Phys. Chem. A* **1998**, *102*, 7787−7794.

(56) Kelly, C. P.; Cramer, C. J.; Truhlar, D. G. Aqueous Solvation Free Energies of Ions and Ion−Water Clusters Based on an Accurate Value for the Absolute Aqueous Solvation Free Energy of the Proton. *J. Phys. Chem. B* **2006**, *110*, 16066−16081.

(57) Konezny, S. J.; Doherty, M. D.; Luca, O. R.; Crabtree, R. H.; Soloveichik, G. L.; Batista, V. S. Reduction of Systematic Uncertainty in DFT Redox Potentials of Transition-Metal Complexes. *J. Phys. Chem. C* **2012**, *116*, 6349−6356.

(58) Isse, A. A.; Gennaro, A. Absolute Potential of the Standard Hydrogen Electrode and the Problem of Interconversion of Potentials in Different Solvents. *J. Phys. Chem. B* **2010**, *114*, 7894−7899.

(59) Marenich, A. V.; Ho, J.; Coote, M. L.; Cramer, C. J.; Truhlar, D. G. Computational Electrochemistry: Prediction of Liquid-Phase

DOI: 10.1021/acscatal.8b02466
ACS Catal. 2018, 8, 7952−7960

Reduction Potentials. *Phys. Chem. Chem. Phys.* **2014**, *16*, 15068−15106.
(60) Marenich, A. V.; Majumdar, A.; Lenz, M.; Cramer, C. J.; Truhlar, D. G. Construction of Pourbaix Diagrams for Ruthenium-Based Water-Oxidation Catalysts by Density Functional Theory. *Angew. Chem., Int. Ed.* **2012**, *51*, 12810−12814.
(61) Hedegård, E. D.; Ryde, U. Molecular Mechanism of Lytic Polysaccharide Monooxygenases. *Chem. Sci.* **2018**, *9*, 3866−3880.
(62) Cao, L.; Caldararu, O.; Rosenzweig, A. C.; Ryde, U. Quantum Refinement Does Not Support Dinuclear Copper Sites in Crystal Structures of Particulate Methane Monooxygenase. *Angew. Chem., Int. Ed.* **2018**, *57*, 162−166.
(63) Michaelos, T. K.; Lant, H. M. C.; Sharninghausen, L. S.; Craig, S. M.; Menges, F. S.; Mercado, B. Q.; Brudvig, G. W.; Crabtree, R. H. Catalytic Oxygen Evolution from Manganese Complexes with an Oxidation-Resistant N, N, O-Donor Ligand. *ChemPlusChem* **2016**, *81*, 1129−1132.
(64) Matheu, R.; Neudeck, S.; Meyer, F.; Sala, X.; Llobet, A. Foot of the Wave Analysis for Mechanistic Elucidation and Benchmarking Applications in Molecular Water Oxidation Catalysis. *ChemSusChem* **2016**, *9*, 3361−3369.
(65) Coggins, M. K.; Zhang, M. T.; Chen, Z.; Song, N.; Meyer, T. J. Single-Site Copper(II) Water Oxidation Electrocatalysis: Rate Enhancements with HPO_4^{2-} as a Proton Acceptor at pH 8. *Angew. Chem., Int. Ed.* **2014**, *53*, 12226−12230.
(66) Yu, F.; Li, F.; Hu, J.; Bai, L.; Zhu, Y.; Sun, L. Electrocatalytic Water Oxidation by a Macrocyclic Cu(II) Complex in Neutral Phosphate Buffer. *Chem. Commun.* **2016**, *52*, 10377−10380.
(67) Chen, F.; Wang, N.; Lei, H.; Guo, D.; Liu, H.; Zhang, Z.; Zhang, W.; Lai, W.; Cao, R. Electrocatalytic Water Oxidation by a Water-Soluble Copper(II) Complex with a Copper-Bound Carbonate Group Acting as a Potential Proton Shuttle. *Inorg. Chem.* **2017**, *56*, 13368−13375.
(68) Shen, J.; Wang, M.; Zhang, P.; Jiang, J.; Sun, L. Electrocatalytic Water Oxidation by Copper(II) Complexes Containing a Tetra-or Pentadentate Amine-Pyridine Ligand. *Chem. Commun.* **2017**, *53*, 4374−4377.
(69) Huang, H.-H.; Wang, J.-W.; Sahoo, P.; Zhong, D.-C.; Lu, T.-B. Electrocatalytic Water Oxidation by Cu(II) Ions in a Neutral Borate Buffer Solution. *Chem. Commun.* **2017**, *53*, 9324−9327.
(70) Bigeleisen, J.; Mayer, M. G. Calculation of Equilibrium Constants for Isotopic Exchange Reactions. *J. Chem. Phys.* **1947**, *15*, 261−267.
(71) Bigeleisen, J.; Wolfsberg, M. Theoretical and Experimental Aspects of Isotope Effects in Chemical Kinetics. *Adv. Chem. Phys.* **2007**, *1*, 15−76.

DOI: 10.1021/acscatal.8b02466
ACS Catal. 2018, 8, 7952−7960